J. Phys. B: At. Mol. Opt. Phys. 27 (1994) 5257–5270. Printed in the UK

Single-centred calculations of excitation and electron removal in intermediate energy p + He^+ collisions

K A Hall, J F Reading and A L Ford

Center for Theoretical Physics, Physics Department, Texas A&M University, College Station, TX 77843, USA

Received 20 June 1994

Abstract. Single-centred finite Hilbert basis set calculations, using bases with a substantial number of orbitals, have been shown to accurately reproduce excitation and electron removal cross sections for the p + H(1s) and p + H($n = 2$) systems. The present paper extends the method to the p + He^+(1s) and p + He^+($n = 2$) collision systems at incident projectile energies of 25 keV and above. Cross sections for 1s → $2l'$, $3l'$ and $4l'$, 2s and 2p → $3l'$ and $4l'$ excitation and for electron removal from the 1s, 2s and 2p are presented and compared to experiment and to other theoretical calculations.

1. Introduction

In this paper we present theoretical cross sections obtained by performing a large single-centred finite Hilbert basis set (FHBS) calculation of a fast proton incident on the $n = 1$ and $n = 2$ states of He^+. A fast proton, energy 25–500 keV, can be accurately considered as following a straight-line path with fixed speed v_p; if directed at a helium ion such a proton defines a time dependent perturbation which can excite or ionize the system. Target ionization can result in the electron ending in a continuum state or attached to the projectile. The conventional way of approaching this problem therefore is to attempt an expansion of the time dependent wavefunction in a set of basis states centred on both the target and the projectile: a two-centred expansion (TCE) (Bates and McCarroll 1958, Wilets and Gallaher 1966, Shakeshaft 1978, Lin *et al* 1978, Winter 1982).

All FHBS calculations are limited by the practical consideration of keeping the basis size reasonably small; this often translates into keeping only s, p and d states in a TCE calculation. The TCE computational algorithm is slow and complicated since the matrix elements of the Hamiltonian taken between the two centres must be evaluated numerically. Also this system of coupled equations must be diagonalized at each step since the two centred bases are not orthogonal to each other. The advantage of the TCE is that it allows a good reproduction of the clustering of the electron around both the projectile and the target as the collision evolves and provides rapid convergence in the basis set.

A single-centred expansion (SCE) calculation mandates the retention of much higher values of angular momentum l if it is to successfully reproduce this clustering aspect of the collision. An SCE however provides a very simple computational algorithm; and with modern fast computers the angular momentum that has to be introduced into the basis is not the problem it was sometime ago. And higher l values may be necessary anyway in calculations where information is required as to excitation cross sections to and from excited states of the system.

0953-4075/94/215257+14$19.50

In two recent papers the present authors (Ford *et al* 1993a, b) showed that single-centred FHBS calculations yielded accurate excitation and electron removal cross sections, for the $p + H(1s)$ and $p + H(n = 2)$ systems, provided a sufficiently large target-centred basis was used. Converged cross sections, with respect to the underlying basis, were produced for collision energies of 15 keV and above. Recently a two centre atomic orbital close coupling expansion method was used (Chen *et al* 1994) to study the p+H(2s) excitation and ionization cross sections. Good agreement with our results was observed for the individual $2s \rightarrow 3l'$ and $4l'$ excitation cross sections.

The present paper reports similar calculations of the $1s \rightarrow 2l'$, $3l'$ and $4l'$, 2s and $2p \rightarrow 3l'$ and $4l'$ excitation and of the electron removal from 1s, 2s and 2p for the single electron $p + He^+$ system. These cross sections are of interest in the field of fusion plasma physics and provide a comparison of theoretical methods with experiment for this basic ion–ion collision system. Although there are extensive experimental results for electron removal from the $He^+(1s)$ initial ground state, we are not aware of any experimental data for the individual sublevel excitation cross sections. We report individual cross sections for the 2s and 2p initial states along with those averaged over all $n = 2$ initial state sublevels.

As in the previous papers we can calculate only total ionization, or electron removal, from the helium system; an SCE method does not allow us to separate processes where the electron is ionized to the continuum from those in which the electron becomes attached to the proton.

A very brief outline of the method is given in section 2. In section 3 we present our results and compare those to experiment and to other calculations.

2. Method

The calculations were carried out using the same methods and basis states used in Ford *et al* (1993a, b). The projectile, which follows a straight-line constant velocity path, $\boldsymbol{R} = (\boldsymbol{B}, v_p t)$, provides a time-dependent perturbation $V(|\boldsymbol{R} - \boldsymbol{r}|, t)$ of the target atom. The state vector $\underline{\psi}_I(t)$, in the interaction picture, is propagated through time using the time-development operator U-matrix approach. This vector $\underline{\psi}_I(t)$ is translated in time by

$$\underline{\psi}_I(t_i) = \mathbf{U}(t_i, t_{i-2})\underline{\psi}_I(t_{i-2}) \approx \exp\left[\frac{-\mathrm{i}}{\hbar v_p}\int_{t_{i-2}}^{t_i} \mathbf{V}_I(t')\mathrm{d}t'\right]\underline{\psi}_I(t_{i-2}). \tag{1}$$

Transition amplitudes constitute the matrix elements of $\mathbf{U}(t_L, -t_L)$, where t_L is some large time where the perturbation $V(|\boldsymbol{R} - \boldsymbol{r}|, t)$ may be neglected. Numerical evaluations of equation (1) are performed using a grid with one t-value between t_{i-2} and t_i. An accurate calculation of each transition amplitude requires an ample number of time grid points and sufficiently small time steps to satisfy the first Magnus approximation.

Using an underlying basis of the form $\phi_{ilm} = r^l e^{-\lambda_i r} Y_{lm}$, where $\lambda_i \in C$, the target Hamiltonian can be diagonalized to produce eigenvector basis states. The basis was constructed with 13 radial functions for each angular momentum value l. For each l pseudostates were produced that represent the low lying bound states and that provide a discrete representation of the continuum. For s partial waves ($l = 0$), our 13 state basis resulted in 5 bound states and 8 continuum states extending up to 1.4 keV above the ionization threshold. The largest angular momentum included, i partial waves ($l = 6$), had 2 bound states and 11 continuum states reaching a maximum of 264 eV above the ionization threshold. A more thorough discussion of the U-matrix approach can be found in Fitchard *et al* (1977) and Ford *et al* (1977).

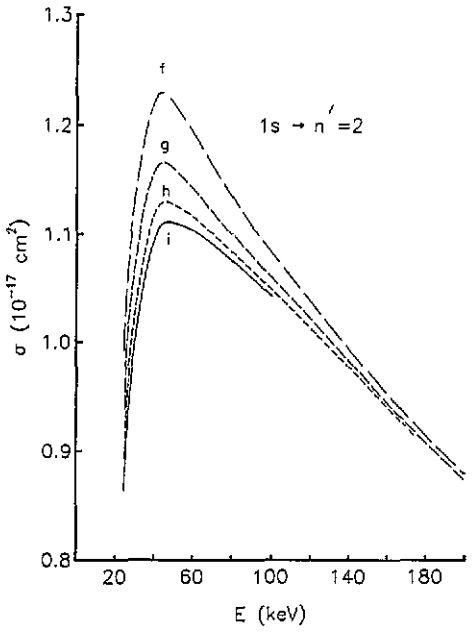

Figure 1. Angular momentum convergence of the $1s \rightarrow n' = 2$ excitation cross section. The curves are labelled with the maximum l used in the basis. Note that the vertical scale does not begin at zero.

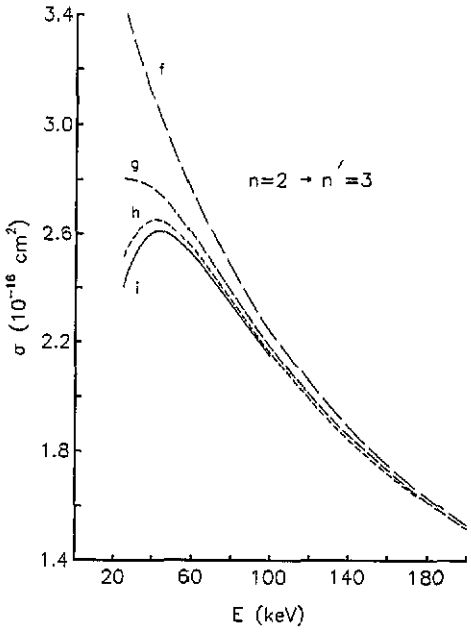

Figure 2. Angular momentum convergence of the $n = 2 \rightarrow n' = 3$ excitation cross section. The curves are labelled with the maximum l used in the basis. Note that the vertical scale does not begin at zero.

3. Results

Several convergence tests have been performed to gauge the accuracy of the target-centred basis results. One test is the convergence in l_{max}, the maximum angular momentum l included in the underlying basis. As the collision energy is decreased, and the charge transfer cross section increases, a higher l_{max} is necessary to adequately describe projectile-centred orbitals for maximum projectile–target separations. Figure 1 shows the l-convergence for the $1s \rightarrow n' = 2$ excitation cross section as a function of projectile collision energy. At the collision energy of 60 keV ($v_p = 0.775$) the $l_{max} = 6$ (i states included), $l_{max} = 5$ (h states included) and $l_{max} = 4$ (g states included) results indicate an l-convergence of 1% for $l_{max} = 6$ and 2% for $l_{max} = 5$. For the lowest energy reported, 25 keV ($v_p = 0.500$), the associated l-convergence is 3% for $l_{max} = 6$ and 5% for $l_{max} = 5$. Similar l-convergence is found for all $1s \rightarrow n'\, l'$ excitation transitions for $n' = 2$, 3 and 4. The l-convergence for the $n = 2 \rightarrow n' = 3$ excitation cross section is shown in figure 2. A similar comparison indicates, for 60 keV, an l-convergence of 1% for $l_{max} = 6$ and 2% for $l_{max} = 5$. As indicated in figure 2 the l-convergence begins to break down at 25 keV with 4.5% for $l_{max} = 6$ and 11% for $l_{max} = 5$. Similar l-convergence results were obtained for the $n = 2 \rightarrow n' = 4$ excitation cross sections. Figure 3 shows the l-convergence for the $He^+(1s)$ electron removal cross section. These single-centred calculations do not compute the separate capture and ionization components of the electron removal cross section, only their sum. A comparison between l_{max} calculations indicates a convergence in angular momentum of 3% for $l_{max} = 6$ and 5.5% for $l_{max} = 5$ at the incident projectile energy of 60 keV. For the lowest energy reported, 25 keV, the associated l-convergence is 12% for $l_{max} = 6$ and 19% for $l_{max} = 5$.

Convergence with respect to the number of time grid points has also been investigated.

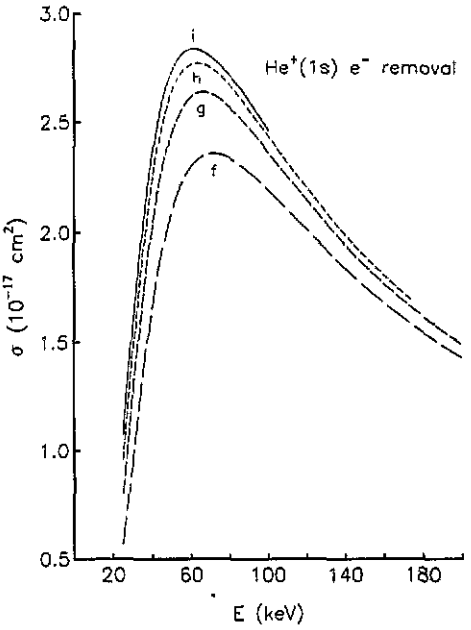

Figure 3. Angular momentum convergence of the $He^+(1s)$ electron removal cross section. The curves are labelled with the maximum l used in the basis. Note that the vertical scale does not begin at zero.

A comparison of calculations using 181, 261 and 341 points indicates that the coupled-state excitation cross sections are converged to within 9% or less at 25 keV but to within less than 3% at collision energies of 60 keV and above. A compilation of these results for incident projectile energies of $E = 25$, 50 and 75 keV is presented in table 1. The convergence with respect to angular momentum and the number of time integration points is given for the $1s \rightarrow n' = 2$, 3 and 4, the $n = 2 \rightarrow n' = 3$ and 4 and the electron removal from the 1s and $n = 2$. The first column indicates the percentage change in the cross section σ when the underlying basis is increased from $l_{max} = 4$ (g states) to $l_{max} = 5$ (h states). The second column reports the change in σ when l_{max} is increased from $l_{max} = 5$ to $l_{max} = 6$. The percentage change in σ when the number of time integration points is increased from 181 to 341, for an $l_{max} = 6$ basis calculation, is presented in the third column. The $1s \rightarrow n'$ and $n = 2 \rightarrow n'$ cross sections are, in general, better converged than the individual 1s and $2l \rightarrow n'l'$ cross sections, with the largest error associated with the smallest cross sections. Our results, for electron removal, from table 1 indicate that the 1s electron removal cross section is only converged to within 21% at 25 keV but to within 6% at 60 keV. The 2s electron removal cross section is converged to within 11% at 25 keV and to within 4% at 60 keV. The 2p and the $n = 2$ electron removal cross sections are converged to within 11% at 25 keV and 4% at 60 keV. We were unable to obtain suitable converged results for energies below 25 keV with the current algorithm. The convergence in l_{max} and also in the number of time integration mesh points appears to be the difficulty.

For the p+H calculations of Ford *et al* (1993a, b) the lowest energy at which reasonable convergence could be obtained was 15 keV. The projectile velocity to 1s electron velocity ratio at 15 keV for $p + H$ is the same as for 60 keV $p + He^+$, so the single-centred method was found to enable converged results at lower scaled energies for this more asymmetric collision. Another significant difference between the $p + H$ and $p + He^+$ systems is that for the former the $1s \rightarrow 1s$ capture is resonant and the cross section becomes large as the collision energy is lowered whereas for the latter it is the $He^+(2s) \rightarrow H(1s)$ capture that is resonant.

Cross sections for $1s \rightarrow 2l'$, $3l'$ and $4l'$ are presented in tables 2 to 4 respectively. The

Table 1. Convergence in l_{max} and the number of time integration points for excitation and electron removal cross sections. The first column indicates the change in σ due to increasing the underlying basis from $l_{max} = 4$ (g states) to $l_{max} = 5$ (h states). The second column shows the variation in σ effected by increasing the basis from $l_{max} = 5$ (h states) to $l_{max} = 6$ (i states). The deviation in an $l_{max} = 6$ calculation of σ, produced by increasing the number of time integration points from 181 to 341, is presented in the third column.

	$l_{max} = 5$	$l_{max} = 6$	341 points
$E = 25$ keV ($v_p = 0.500$)			
$1s \rightarrow n' = 2$	−4.8%	−3.3%	4.9%
$1s \rightarrow n' = 3$	−13.6%	−9.9%	5.5%
$1s \rightarrow n' = 4$	−17.4%	−12.7%	5.9%
$n = 2 \rightarrow n' = 3$	−10.4%	−4.5%	4.1%
$n = 2 \rightarrow n' = 4$	−19.4%	−8.2%	3.6%
$He^+(1s)$ e^- removal	19.0%	11.8%	8.5%
$He(n = 2)$ e^- removal	18.2%	7.3%	2.8%
$E = 50$ keV ($v_p = 0.707$)			
$1s \rightarrow n' = 2$	−2.8%	−1.5%	2.1%
$1s \rightarrow n' = 3$	−6.2%	−3.1%	2.4%
$1s \rightarrow n' = 4$	−8.0%	−4.3%	2.4%
$n = 2 \rightarrow n' = 3$	−2.8%	−1.2%	2.4%
$n = 2 \rightarrow n' = 4$	−6.1%	−1.7%	2.7%
He(1s) e^- removal	7.5%	3.6%	3.5%
$He(n = 2)$ e^- removal	8.5%	2.1%	1.5%
$E = 75$ keV ($v_p = 0.866$)			
$1s \rightarrow n' = 2$	−1.5%	−0.8%	1.9%
$1s \rightarrow n' = 3$	−2.7%	−1.4%	2.2%
$1s \rightarrow n' = 4$	−3.6%	−1.8%	2.3%
$n = 2 \rightarrow n' = 3$	−1.3%	−0.8%	1.2%
$n = 2 \rightarrow n' = 4$	−2.2%	−1.0%	2.2%
He(1s) e^- removal	4.2%	2.0%	3.0%
$He(n = 2)$ e^- removal	6.1%	1.7%	1.6%

Table 2. Cross sections for $1s \rightarrow 2l'$ excitation (in units of 10^{-18} cm^2) as a function of the collision energy. Also the approach of the $1s \rightarrow 2l'$ excitation cross sections to the first Born as the collision energy E is increased. For $E \geqslant 200$ keV the cross section σ (in units of 10^{-18} cm^2) and the per cent deviation from the first Born, $\Delta = (\sigma - \sigma_{Born})/\sigma_{Born}$, are given. The 2p cross sections are summed over all the degenerate sublevels of the final state.

	25 keV	40 keV	60 keV	75 keV	100 keV	125 keV	150 keV	175 keV
$1s \rightarrow 2s$	5.80	6.24	4.77	3.89	2.92	2.33	1.92	1.63
$1s \rightarrow 2p$	2.85	4.71	6.27	6.94	7.50	7.71	7.66	7.50
$1s \rightarrow n' = 2$	8.65	11.0	11.0	10.8	10.4	10.0	9.58	9.13

	200 keV		250 keV		300 keV		400 keV		500 keV	
	σ	Δ	σ	Δ	σ	Δ	σ	Δ	σ	Δ
$1s \rightarrow 2s$	1.42	36%	1.12	29%	0.916	25%	0.672	19%	0.529	16%
$1s \rightarrow 2p$	7.32	−12%	6.87	−9.1%	6.43	−7.3%	5.68	−5.2%	5.08	−3.9%
$1s \rightarrow n' = 2$	8.74	−6.4%	7.98	−5.1%	7.35	−4.2%	6.35	−3.1%	5.61	−2.4%

2s and 2p $\rightarrow 3l'$ and $4l'$ cross sections are presented in tables 5 and 6. The $2l \rightarrow n'l'$ cross sections are summed over final state m' values and averaged over the initial state m values,

Table 3. *Cross sections for* $1s \rightarrow 3l'$ *excitation* (*in units of* 10^{-19} cm^2) as a function of the collision energy. Also the approach of the $1s \rightarrow 3l'$ excitation cross sections to the first Born as the collision energy E is increased. Δ is the per cent deviation from the first Born, as in table 2. The 3p and 3d cross sections are summed over all the degenerate sublevels of the final state.

	25 keV	40 keV	60 keV	75 keV	100 keV	125 keV	150 keV	175 keV
$1s \rightarrow 3s$	6.19	12.2	11.1	9.30	7.00	5.52	4.48	3.75
$1s \rightarrow 3p$	6.65	8.24	10.1	11.3	12.6	13.1	13.2	12.9
$1s \rightarrow 3d$	1.35	1.73	2.26	2.41	2.37	2.20	2.00	1.80
$1s \rightarrow n'=3$	14.2	22.2	23.5	23.0	21.9	20.9	19.6	18.5

	200 keV		250 keV		300 keV		400 keV		500 keV	
	σ	Δ	σ	Δ	σ	Δ	σ	Δ	σ	Δ
$1s \rightarrow 3s$	3.22	55%	2.48	44%	2.00	37%	1.44	28%	1.11	22%
$1s \rightarrow 3p$	12.7	−13%	11.9	−9.6%	11.1	−7.6%	9.81	−5.2%	8.75	−3.9%
$1s \rightarrow 3d$	1.63	28%	1.36	24%	1.16	21%	0.886	16%	0.715	12%
$1s \rightarrow n'=3$	17.5	−1.9%	15.7	−1.5%	14.3	−1.2%	12.1	−0.9%	10.6	−0.7%

Table 4. Cross sections for $1s \rightarrow 4l'$ excitation (in units of 10^{-19} cm^2) as a function of the collision energy. Also the approach of the $1s \rightarrow 4l'$ excitation cross sections to the first Born as the collision energy E is increased. Δ is the percent deviation from the first Born, as in table 2. The 4p, 4d and 4f cross sections are summed over all the degenerate sublevels of the final state.

	25 keV	40 keV	60 keV	75 keV	100 keV	125 keV	150 keV	175 keV
$1s \rightarrow 4s$	1.13	3.93	4.25	3.71	2.83	2.23	1.80	1.50
$1s \rightarrow 4p$	2.59	3.24	3.56	3.92	4.34	4.58	4.62	4.56
$1s \rightarrow 4d$	0.857	0.904	1.08	1.15	1.12	1.04	0.954	0.860
$1s \rightarrow 4f$	0.10	0.10	0.11	0.096	0.070	0.055	0.044	0.035
$1s \rightarrow n'=4$	4.68	8.17	8.99	8.87	8.36	7.91	7.41	6.95

	200 keV		250 keV		300 keV		400 keV		500 keV	
	σ	Δ	σ	Δ	σ	Δ	σ	Δ	σ	Δ
$1s \rightarrow 4s$	1.28	65%	0.973	53%	0.779	44%	0.551	32%	0.425	25%
$1s \rightarrow 4p$	4.48	−14%	4.22	−10%	3.95	−8.2%	3.48	−5.5%	3.11	−4.1%
$1s \rightarrow 4d$	0.777	29%	0.645	24%	0.548	20%	0.420	16%	0.339	12%
$1s \rightarrow 4f$	0.028	140%	0.020	100%	0.015	82%	0.0099	55%	0.0073	40%
$1s \rightarrow n'=4$	6.56	−0.2%	5.85	−0.3%	5.29	−0.3%	4.46	−0.2%	3.88	−0.2%

$$\sigma(2l \rightarrow n'l') = \left(\frac{1}{2l+1}\right) \sum_m \sum_{m'} \sigma(2lm \rightarrow n'l'm'). \tag{2}$$

The $\sigma(2l \rightarrow n')$ cross sections are given by

$$\sigma(2l \rightarrow n') = \sum_{l'} \sigma(2l \rightarrow n'l') \tag{3}$$

while the $\sigma(n=2 \rightarrow n')$ cross sections are averaged over the initial state l value,

$$\sigma(n=2 \rightarrow n') = \tfrac{1}{4}\left(\sigma(2s \rightarrow n') + 3\,\sigma(2p \rightarrow n')\right). \tag{4}$$

Individual $\sigma(1s \rightarrow n'l'm')$ and $\sigma(2lm \rightarrow n'l'm')$ cross sections have been tabulated and can be provided upon request. In addition to listing the individual excitation cross sections,

Table 5. Cross sections for 2s and 2p → 3l' excitation (in units of 10^{-17} cm^2) as a function of the collision energy. Also the approach of the 2s and 2p → 3l' excitation cross sections to the first Born as the collision energy E is increased. Δ is the percent deviation from the first Born, as in table 2. In each case the cross sections are summed over all the degenerate sublevels of the indicated final state and averaged over the degenerate sublevels of the initial state.

	25 keV	40 keV	60 keV	75 keV	100 keV	125 keV	150 keV	175 keV
2s → 3s	4.37	4.38	3.81	3.35	2.72	2.27	1.93	1.67
2s → 3p	4.40	5.77	6.98	7.35	7.43	7.26	6.96	6.67
2s → 3d	15.5	14.4	11.8	10.2	8.21	6.86	5.86	5.13
2s → $n' = 3$	24.2	24.5	22.6	20.9	18.4	16.4	14.8	13.5
2p → 3s	0.823	0.608	0.456	0.391	0.325	0.287	0.260	0.240
2p → 3p	7.24	6.17	4.80	4.03	3.14	2.56	2.15	1.85
2p → 3d	15.9	19.8	20.8	20.4	19.0	17.7	16.4	15.2
2p → $n' = 3$	23.9	26.6	26.1	24.8	22.5	20.5	18.8	17.3
$n = 2 \rightarrow n' = 3$	24.0	26.1	25.2	23.8	21.5	19.5	17.8	16.4

	200 keV		250 keV		300 keV		400 keV		500 keV	
	σ	Δ	σ	Δ	σ	Δ	σ	Δ	σ	Δ
2s → 3s	1.47	5.6%	1.19	5.3%	0.992	4.9%	0.744	4.2%	0.594	3.5%
2s → 3p	6.37	−11%	5.76	−8.3%	5.25	−6.7%	4.46	−4.7%	3.87	−3.6%
2s → 3d	4.54	2.3%	3.66	2.3%	3.06	2.2%	2.30	1.9%	1.84	1.7%
2s → $n' = 3$	12.4	−4.5%	10.6	−3.4%	9.30	−2.7%	7.50	−1.9%	6.31	−1.5%
2p → 3s	0.223	−5.9%	0.196	−5.3%	0.175	−4.7%	0.146	−3.7%	0.126	−3.0%
2p → 3p	1.62	5.4%	1.30	4.6%	1.08	3.9%	0.808	3.0%	0.645	2.4%
2p → 3d	14.2	−7.5%	12.5	−5.7%	11.2	−4.6%	9.22	−3.2%	7.88	−2.4%
2p → $n' = 3$	16.1	−6.4%	14.0	−4.8%	12.4	−3.9%	10.2	−2.7%	8.65	−2.1%
$n = 2 \rightarrow n' = 3$	15.2	−6.0%	13.1	−4.6%	11.6	−3.7%	9.51	−2.6%	8.06	−2.0%

tables 2–6 also show the approach of these cross sections to the first Born approximation. The dipole forbidden transitions approach the first Born much more slowly than do the dipole allowed ones for the 1s → 2l' and 3l' excitation cross sections. The 1s → n's and 1s → n'd cross sections approach the first Born from above and the 1s → n'p cross sections approach the first Born from below, so the 1s → $n' = 2$ and 1s → $n' = 3$ summed cross sections approach the first Born more rapidly than do the individual $n'l'$ cross sections. The 1s → 4f cross section is much smaller than the other $n' = 4$ cross sections. The cross sections for the $n = 2$ initial state are closer to the first Born at each energy than are the $n = 1$ cross sections.

Our results for 1s → 2s, 2p and $n' = 2$ excitation are compared to three TCE calculations (Bransden and Noble 1981, Bransden *et al* 1983) and an analytic fit to calculated cross sections (Cohen 1988) in figures 4, 5 and 6 respectively. Krstic and Janev (1993) have recently published results for the 1s → $n' = 2$ and $n' = 3$ and the $n = 2 \rightarrow n' = 3$ and $n' = 4$ excitation cross sections. These calculations were carried out using an adiabatic coupled molecular state model applicable to slow atomic collisions. Their results for 1s → $n' = 2$ excitation, for projectile energies of 25–60 keV (Krstic 1994), are also included in figure 6.

The calculations of Bransden and Noble (1981) present a four-state basis set centred on both the target and projectile. The calculations of Bransden *et al* (1983) present alternative basis TCE calculations using a 19-state basis set centred on the projectile with a four-state set on the target and a 19-state basis set centred on the target with a four-state set on the projectile. Low energy results, projectile energies below 25 keV, are also shown for comparison. These low energy results were carried out using a coupled molecular state

Table 6. Cross sections for 2s and 2p → $4l'$ excitation (in units of 10^{-17} cm^2) as a function of the collision energy. Also the approach of the 2s and 2p → $4l'$ excitation cross sections to the first Born as the collision energy E is increased. Δ is the percent deviation from the first Born, as in table 2. In each case the cross sections are summed over all the degenerate sublevels of the indicated final state and averaged over the degenerate sublevels of the initial state.

	25 keV	40 keV	60 keV	75 keV	100 keV	125 keV	150 keV	175 keV
2s → 4s	1.00	0.985	0.858	0.749	0.598	0.491	0.413	0.355
2s → 4p	0.942	0.981	1.19	1.27	1.31	1.29	1.25	1.20
2s → 4d	2.09	1.74	1.43	1.23	0.997	0.835	0.720	0.628
2s → 4f	2.34	1.92	1.34	1.06	0.761	0.592	0.480	0.409
2s → $n'=4$	6.37	5.63	4.82	4.31	3.66	3.21	2.86	2.59
2p → 4s	0.208	0.145	0.105	0.0866	0.0685	0.0586	0.0520	0.0474
2p → 4p	1.82	1.45	1.08	0.888	0.672	0.538	0.446	0.381
2p → 4d	2.50	3.05	3.21	3.13	2.90	2.67	2.46	2.27
2p → 4f	1.58	1.55	1.29	1.10	0.871	0.717	0.601	0.520
2p → $n'=4$	6.11	6.20	5.68	5.21	4.51	3.99	3.56	3.22
$n=2 \rightarrow n'=4$	6.17	6.06	5.47	4.98	4.30	3.79	3.39	3.06

	200 keV		250 keV		300 keV		400 keV		500 keV	
	sigma	Δ	σ	Δ	σ	Δ	σ	Δ	σ	Δ
2s → 4s	0.310	13%	0.246	11%	0.204	9.9%	0.151	7.8%	0.120	6.3%
2s → 4p	1.14	−12%	1.04	−9.0%	0.950	−7.2%	0.810	−5.0%	0.706	−3.8%
2s → 4d	0.554	−1.6%	0.448	−0.8%	0.376	−0.3%	0.284	0.1%	0.228	0.3%
2s → 4f	0.348	16%	0.269	12%	0.219	9.5%	0.160	6.4%	0.126	4.7%
2s → $n'=4$	2.36	−3.2%	2.00	−2.5%	1.75	−2.1%	1.40	−1.5%	1.18	−1.2%
2p → 4s	0.0435	−6.1%	0.0377	−5.6%	0.0335	−5.0%	0.0277	−4.0%	0.0238	−3.3%
2p → 4p	0.331	9.2%	0.263	7.4%	0.217	6.1%	0.161	4.4%	0.128	3.4%
2p → 4d	2.12	−7.2%	1.85	−5.4%	1.64	−4.2%	1.35	−2.9%	1.15	−2.2%
2p → 4f	0.455	17%	0.360	13%	0.297	11%	0.220	8.1%	0.174	6.2%
2p → $n'=4$	2.95	−2.4%	2.51	−1.8%	2.19	−1.4%	1.76	1.0%	1.47	−0.8%
$n=2 \rightarrow$ $n'=4$	2.80	−2.6%	2.38	−2.0%	2.08	−1.6%	1.67	−1.1%	1.40	−0.9%

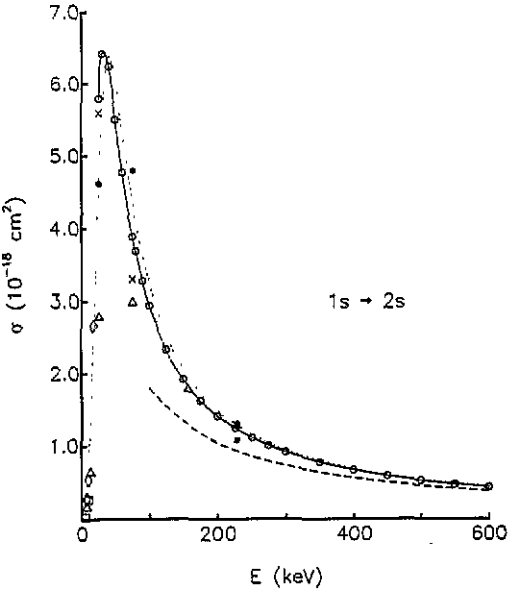

Figure 4. The excitation cross section for 1s → 2s as a function of incident projectile energy. The full curve represents the present single-centred results with the open circles (○) being the calculated points. The first Born result is represented by the broken curve. The dotted curve is an analytic fit by Cohen (1988). The open triangles (△) are the TCE calculations of Bransden and Noble (1981); a four-state set centred on both the target and projectile. The crosses (×) and full circles (●) represent alternative basis TCE calculations by Bransden *et al* (1983). Calculations using a 19-state set centred on the projectile with a four-state set on the target are given by the full circles (●). The crosses (×) represent calculations using a 19-state set centred on the target and a four-state set on the projectile. Low energy molecular state calculations are represented by the open diamonds (◇) (Winter *et al* 1980) and the open squares (□) (Kimura and Thorson 1981).

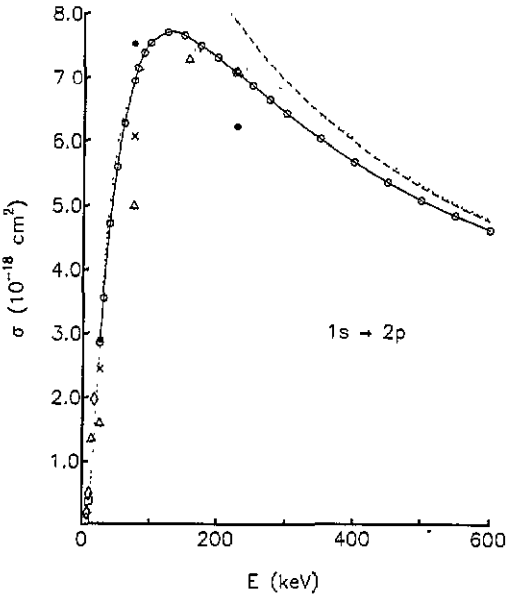

Figure 5. The excitation cross section for 1s → 2p as a function of incident projectile energy. The same notation as in figure 4 is used.

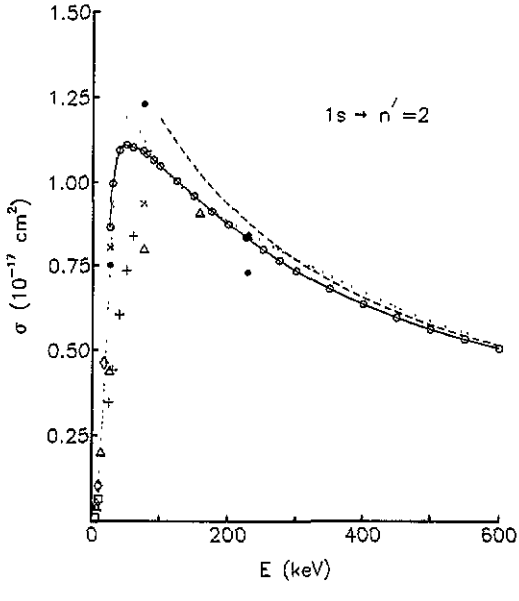

Figure 6. The excitation cross section for 1s → $n' = 2$ as a function of incident projectile energy. The same notation as in figure 4 is used. In addition the adiabatic results (+) of Krstic and Janev (1993) are shown in the energy range of 25–60 keV (Krstic 1994).

basis (Winter *et al* 1980, Kimura and Thorson 1981). The results of Cohen (1988) represent analytic fits to the calculations of Bransden *et al* (1983), Kimura and Thorson (1981) and Winter *et al* (1980) with extrapolations to higher energies using the Born approximation (Bates and Griffing 1953). Our results are in very good agreement with the different basis TCE results (Bransden and Noble 1981, Bransden *et al* 1983) at the higher energies, but still where the differences from the first Born are significant. Our results at 75.5 keV, for each cross section, lie between the two TCE results using the larger 23-state bases. The 8-state results (Bransden and Noble 1981) are below our results, for each cross section, except at their highest reported energy of 227.5 keV. Their calculation was not done at enough energies to clearly define the cross section peak. Though the fit to these TCE calculations

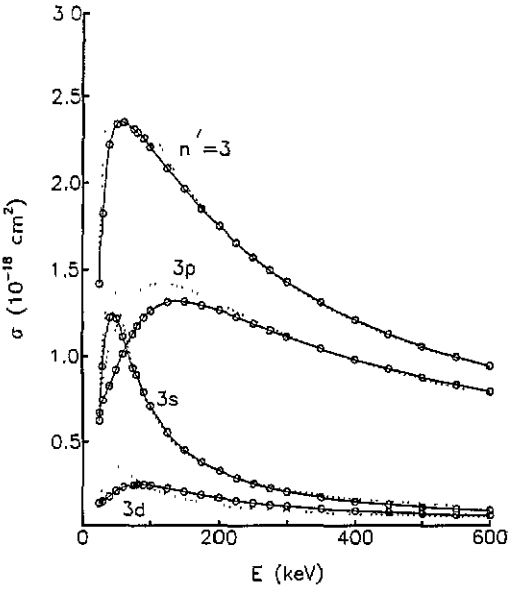

Figure 7. The excitation cross sections for 1s → 3s, 3p, 3d and $n' = 3$ as a function of incident projectile energy. The full curves represent the present single-centred results with the open circles (O) being the calculated points. The dotted curves are the least-squares analytic fits, of their calculated Sturmian basis results, reported by Stodden *et al* (1990).

by Cohen (1988) is in excellent agreement with our results over the 25–227.5 keV energy range, our results indicate that this fit approaches the Born approximation too quickly for the 1s → 2p and $n' = 2$ excitation cross sections. A comparison of our results with those of the adiabatic model (Krstic and Janev 1993, Krstic 1994) implies a lack of correspondence between these two techniques. Our 1s → $n' = 2$ cross sections are a factor of 2.5 and 1.3 greater at 25 keV and 60 keV respectively. The endpoints of this energy domain, 25 keV and 60 keV, denote the currently reported lower (SCE) and upper (adiabatic model) limits of these two methods.

Our excitation cross section results for 1s → 3s, 3p, 3d and $n' = 3$ and presented in figure 7 along with comparisons to the Sturmian basis results of Stodden *et al* (1990). Our results indicate excellent agreement with the Stodden *et al* (1990) results except at the peaks for these $n' = 3$ sublevel cross sections. A 15% difference between our results at the $n' = 3$ peak indicates the general disagreement between the cross section peaks of the various sublevel excitation results.

In figures 8 and 9 we present a comparison between our 1s → $n' = 3$ and $n' = 4$ and $n = 2 \rightarrow n' = 3$ and $n' = 4$ excitation results with the classical calculations of Cohen (1988) and the adiabatic method computations of Krstic and Janev (1993). The Cohen (1988) calculations of the 1s → $n' = 3$ and $n = 2 \rightarrow n' = 3$ and $n' = 4$ excitation cross section were calculated using a classical-trajectory Monte Carlo (CTMC) method. The 1s → $n' = 4$ excitation cross section was calculated using a modified classical binary-encounter model. The cross sections for 1s → $n' = 3$ and $n' = 4$ excitation, presented in figure 8, are both in disagreement with those of Cohen (1988), whereas the excited target state cross sections, $n = 2 \rightarrow n' = 3$ and $n' = 4$, presented in figure 9, are in excellent accord with the CTMC results over the entire energy range of 25–600 keV. We are unable to explain this discrepancy between our results and the CTMC and binary-encounter results for the 1s → $n' = 3$ and 1s → $n' = 4$ excitation respectively. As already noted, the results of Stodden *et al* (1990) for 1s → $n' = 3$ excitation are in general agreement with ours and thus are also in disagreement with the CTMC results of Cohen for this particular excitation cross section. The adiabatic model results (Krstic and Janev 1993, Krstic 1994) are depicted in figures 8 and 9 for projectile energies of 25–60 keV. We observe a general

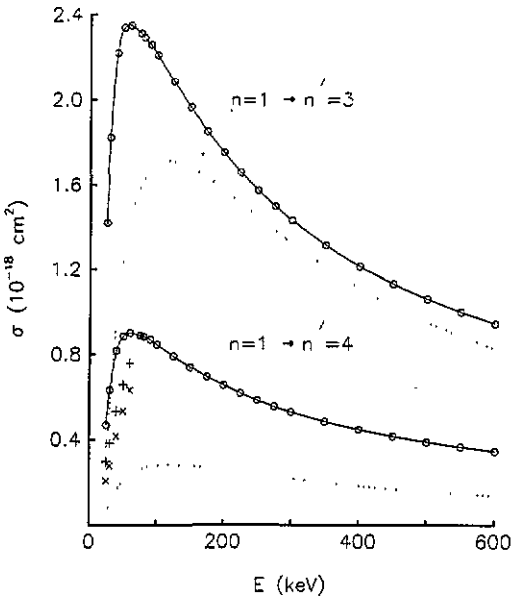

Figure 8. The excitation cross sections for $1s \rightarrow n' = 3$ and $1s \rightarrow n' = 4$ as a function of incident projectile energy. The full curves represent the present single-centred results with the open circles (O) being the calculated points. The dotted lines are classical calculations by Cohen (1988). The $1s \rightarrow n' = 3$ curve was determined using a classical- trajectory Monte Carlo (CTMC) method while the $1s \rightarrow n' = 4$ result was obtained using a classical binary-encounter model. The adiabatic results of Krstic and Janev (1993), $1s \rightarrow n' = 3$ (+) and $1s \rightarrow n' = 4$ (×), are shown in the energy range of 25–60 keV (Krstic 1994).

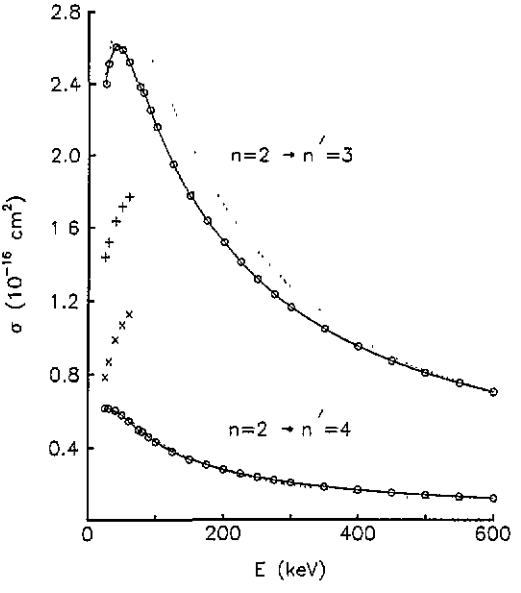

Figure 9. The excitation cross sections for $n = 2 \rightarrow n' = 3$ and $n' = 4$ as a function of incident projectile energy. The full curves represent the present single-centred results with the open circles (O) being the calculated points. The dotted curves are the classical-trajectory Monte Carlo (CTMC) results of Cohen (1988). The adiabatic results of Krstic and Janev (1993), $n = 2 \rightarrow n' = 3$ (+) and $n = 2 \rightarrow n' = 4$ (×), are shown in the energy range of 25–60 keV (Krstic 1994).

lack of agreement between our SCE results and these adiabatic model calculations. The $n = 1 \rightarrow n' = 4$ excitation results are in closest agreement with our cross sections being 2.3 and 1.4 larger at 25 keV and 60 keV respectively. Our reported excitation cross sections are larger than these adiabatic results except for the $n = 2 \rightarrow n' = 4$ excitation reaction. For this particular reaction our SCE results are smaller by a factor of 1.3 and 2.0 at 25 keV and 60 keV respectively.

A compilation of our results for electron removal from $He^+(1s)$, $He^+(2l)$ and $He^+(n = 2)$ is given in table 7. Figure 10 presents a comparison of our $He^+(1s)$ electron removal cross section with those of experiment and theory. There have been a number of previous calculations of the ionization and charge transfer cross sections for the $He^+(1s)$ initial state.

Table 7. Cross sections for electron removal from $He^+(1s)$, $He^+(2s)$ and $He^+(2p)$ (in units of 10^{-17} cm^2) as a function of the collision energy. For the 2p initial state the cross section is averaged over the three m components of this state. The averaging over the initial state gives $\sigma(n=2) = \frac{1}{4}(\sigma(2s) + 3\sigma(2p))$. Δ is the per cent deviation from the first Born, as in table 2.

	25 keV	40 keV	60 keV	75 keV	100 keV	125 keV	150 keV	175 keV
$\sigma(1s)$	1.07	2.36	2.84	2.76	2.46	2.15	1.89	1.69
$\sigma(2s)$	36.4	26.4	18.0	14.6	11.2	8.81	7.58	6.63
$\sigma(2p)$	45.7	34.3	23.0	18.4	13.8	10.9	9.24	7.99
$\sigma(n=2)$	43.4	32.3	21.8	17.4	13.2	10.4	8.82	7.65

	200 keV		250 keV		300 keV		400 keV		500 keV	
	σ	Δ	σ	Δ	σ	Δ	σ	Δ	σ	Δ
$\sigma(1s)$	1.49	28%	1.25	19%	1.07	14%	0.846	8.4%	0.702	5.5%
$\sigma(2s)$	5.49	−5.2%	4.51	−6.4%	3.84	−7.0%	2.99	−7.7%	2.46	−8.0%
$\sigma(2p)$	6.66	−2.8%	5.40	−4.3%	4.56	−5.1%	3.50	−5.9%	2.85	−6.3%
$\sigma(n=2)$	6.37	−3.3%	5.18	−4.7%	4.38	−5.5%	3.37	−6.3%	2.75	−6.7%

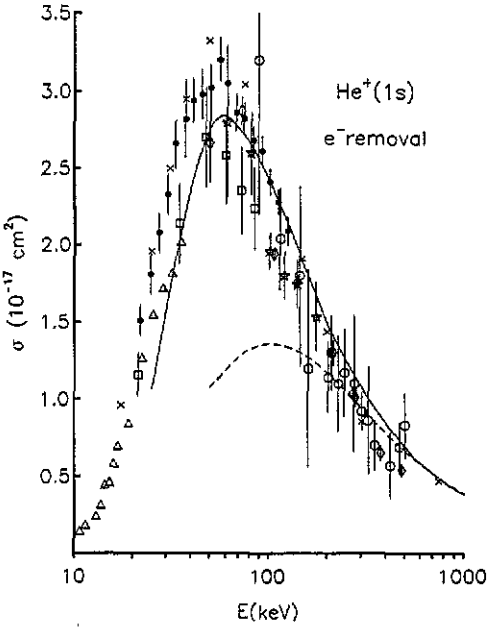

Figure 10. The $He^+(1s)$ electron removal cross section. The full curve is the present single-centred result. The first Born result is represented by the broken curve. Theoretical calculations: ×, coupled-state Sturmian basis (Stodden *et al* 1990). Experimental data: ○, Mitchell *et al* (1977); △, Peart *et al* (1977); ◇, Angel *et al* (1978); □, Peart *et al* (1983); ●, Rinn *et al* (1986); ⋆, Watts *et al* (1986).

In the figure we compare only to the most recent and extensive calculation, that of Stodden *et al* (1990). This paper reported $p + He^+(1s)$ electron removal cross sections for projectile energies of 17.5–750 keV. These stripping cross sections were subsequently scaled and used to study muon-catalysed d–t fusion. Their electron removal results are somewhat larger than ours for energies at and below the cross section maximum and are in better agreement with the recent experimental data of Rinn *et al* (1986). Since the convergence of our results have been carefully checked the reason for this discrepancy is unclear.

Our results for electron removal from $He^+(1s)$ and $He^+(n=2)$ are compared with those of Cohen (1988) in figure 11. The results of Cohen (1988) represent CTMC calculations for the $He^+(n=2)$ electron removal and an analytic fit to experiment (Angel *et al* 1978, Peart *et al* 1977) for the $He^+(1s)$ electron removal. The fit uses experiment for $v < 4$ (au) and the Born approximation for $v > 4$ (au). Our single-centred calculations are in close agreement

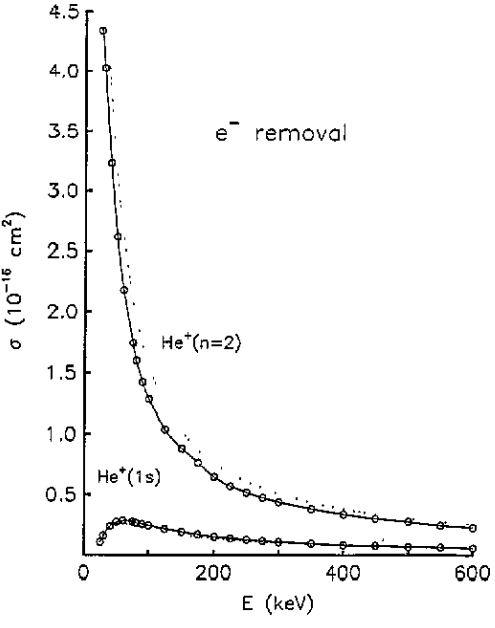

Figure 11. The $He^+(1s)$ and $He^+(n = 2)$ electron removal cross section. The full curves represent the present single-centred results with the open circles (O) being the calculated points. The dotted lines are the results of Cohen (1988): the $He^+(1s)$ result is an analytic fit to experiment (Angel *et al* 1978, Peart *et al* 1977) and the $He^+(n = 2)$ curve represents a CTMC method calculation.

with both of these results. Krstic and Janev (1993) calculate ionization cross sections for the $p + He^+(n = 2)$ system. They report results up to 60 keV but do not include the capture component and thus their results cannot be compared to our electron removal cross sections. We are not aware of any published experimental results for electron removal from the excited state target.

Acknowledgments

This work was supported by a grant from the US National Science Foundation PHY-9318449 and by the US Department of Energy under grant DE-FG05-92ER54174. We thank Predrag Krstic for providing a numerical tabulation of the adiabatic approximation results of Krstic and Janev (1993) and additional results extending up to 60 keV (Krstic 1994). We also would like to thank James S Cohen for providing helpful discussions concerning the results of Cohen (1988).

References

Angel G C, Dunn K F, Sewell E C and H B Gilbody 1978 *J. Phys. B: At. Mol. Phys.* **11** L49–53
Bates D R and Griffing G 1953 *Proc. R. Phys. Soc.* A **66** 961
Bates D R and McCarroll 1958 *Proc. R. Soc.* A **245** 175–85
Bransden B H and Noble C J 1981 *J. Phys. B: At. Mol. Phys.* **14** 1849–56
Bransden B H, Noble C J and Chandler J 1983 *J. Phys. B: At. Mol. Phys.* **16** 4191–201
Chen Z, Esry B D, Lin C D and Piacentini R D 1994 *J. Phys. B: At. Mol. Opt. Phys.* **27** 2511–20
Cohen J S 1988 *Muon Cat. Fus.* **3** 499
Fitchard E, Ford A L and Reading J F 1977 *Phys. Rev.* A **16** 1325–8
Ford A L, Fitchard E, and Reading J F 1977 *Phys. Rev.* A **16** 133–43
Ford A L, Reading J F and Hall K A 1993a *J. Phys. B: At. Mol. Opt. Phys.* **26** 4537–51
—— 1993b *J. Phys. B: At. Mol. Opt. Phys.* **26** 4553–60
Kimura M and Thorson W R 1981 *Phys. Rev.* A **24** 3019–31

Krstic P S 1994 Private communication
Krstic P S and Janev R K 1993 *Phys. Rev.* A **47** 3894–12
Lin C D, Soongand S C and Tunnell L N 1978 *Phys. Rev.* A **17** 1646
Mitchell J B A, Dunn K F, Angel G C, Browning R and Gilbody H B 1977 *J. Phys. B: At. Mol. Phys.* **10** 1897–910
Peart B, Rinn K and Dolder K 1983 *J. Phys. B: At. Mol. Phys.* **16** 1461–9
Peart B, Grey R and Dolder K T 1977 *J. Phys. B: At. Mol. Phys.* **10** 2675–82
Rinn K, Melchert F, Rink K and Salzborn E 1986 *J. Phys. B: At. Mol. Phys.* **19** 3717–26
Shakeshaft R 1978 *Phys. Rev.* A **18** 1930–4
Stodden C D, Monkhorst H J and Szalewicz K 1990 *Phys. Rev.* A **41** 1281–92
Watts M F, Dunn K F and Gilbody H B 1986 *J. Phys. B: At. Mol. Phys.* **19** L355–9
Wilets L and Gallaher D F 1966 *Phys. Rev.* **147** 13–20
Winter T G 1982 *Phys. Rev.* A **25** 697
Winter T G, Hatton G J and Lane N F 1980 *Phys. Rev.* A **22** 930–6